Phase behaviors and self-assembly properties of two catanionic surfactant systems: C8F17COOH/TTAOH/H2O and C 8H17COOH/TTAOH/H2O

ARTICLE *in* THE JOURNAL OF PHYSICAL CHEMISTRY B · OCTOBER 2010

Impact Factor: 3.3 · DOI: 10.1021/jp104579h · Source: PubMed

Phase Behaviors and Self-Assembly Properties of Two Catanionic Surfactant Systems: $C_8F_{17}COOH/TTAOH/H_2O$ and $C_8H_{17}COOH/TTAOH/H_2O$

Juan Zhang,[†] Aixin Song,[†] Zhibo Li,[‡] Guiying Xu,[†] and Jingcheng Hao*[,†]

Key Laboratory of Colloid and Interface Chemistry, Shandong University, Ministry of Education, Jinan 250100, P. R. China, and Beijing National Laboratory for Molecular Sciences, State Key Laboratory of Physical and Chemistry Joint Laboratory Polymer Science and Materials, Institute of Chemistry, Chinese Academy of Sciences, Beijing 100080, P. R. China

Received: May 19, 2010; Revised Manuscript Received: September 5, 2010

Two fatty acids, perfluorononanoic acid ($C_8F_{17}COOH$) and nonanoic acid ($C_8H_{17}COOH$), were mixed with a cationic hydrocarbon surfactant, tetradecyltrimethylammonium hydroxide (TTAOH), in aqueous solutions for comparative investigation. Phase behaviors of the two systems are quite different because of the special properties of the fluorocarbon chains. For the $C_8H_{17}COOH/TTAOH/H_2O$ system, a single L_α phase region with phase transition from planar lamellar phase ($L_{\alpha l}$ phase) to vesicle phase ($L_{\alpha v}$ phase) was observed. For the $C_8F_{17}COOH/TTAOH/H_2O$ system, two single phases consisting of vesicles were obtained at room temperature. One is a high viscoelastic gel phase consisting of vesicles with crystalline state bialyers at the $C_8F_{17}COOH$-rich side, which was confirmed by freeze-fracture transmission electron microscope (FF-TEM) and differential scanning calorimetry (DSC) measurements. With the increase of TTAOH proportion, another vesicle phase consisting of liquid state bilayers was observed after the two-phase region. The fluorosurfactant systems prefer to form vesicle bilayers than the corresponding hydrocarbon ones because of the rigid structure, the stronger hydrophobicity, and the larger volume of fluorocarbon chains.

Introduction

Vesicles that were early described in 1964[1] for lipids in aqueous solution are interesting and important self-assembled structures in scientific research, which have wide-ranging industry applications.[2] Since Kaler et al. reported the thermodynamically stable vesicles in aqueous solutions of single-tailed cationic and anionic (catanionic) surfactant mixtures in 1989,[3] catanionic surfactant mixtures as typical model systems of surfactants in solutions have attracted great attention in constructing self-assembled structures, especially the vesicles.[4−12] However, an undesired phenomenon is often observed. Precipitates often form at equimolecular mixtures because the electrostatic interaction between the charged aggregates, in which is screened by excess salts formed from the counterions of cationic and anionic surfactants. In recent years, extensive studies have been focused on salt-free catanionic surfactant systems.[13−19] Rich phase behaviors and novel aggregates have been observed in these systems due to the absence of salts. To obtain the salt-free catanionic surfactant systems, cationic surfactants with OH^- as counterions were often used to be mixed with anionic ones with H^+ as counterions and salts were avoided because of the formation of H_2O. In these salt-free catanionic surfactant mixtures, vesicles of hydrocarbon mixtures[16,18] have been studied in detail and used to enhance the solubility of fullerene C_{60} in aqueous solution.[19] Recently, stable reverse vesicles of salt-free catanionic surfactant mixtures in nonpolar organic solvents like cyclohexane were prepared,[20,21] which may provide ideal micro- or nanoreaction centers for biological tests to trap guest molecules such as enzymes.[22]

Among the surfactants used to construct self-assembly aggregates, fluorosurfactants have unique physicochemical properties because of the fluorocarbon chains such as high surface activity, hydrophobic and oleophobic properties, and chemical stability, etc. Therefore, the aggregation behaviors of fluorosurfactants in solutions often present differences from those of hydrocarbon surfactants, which trigger a flame in the study of fluorosurfactant systems.[23−26] However, compared to the systematic investigations of the corresponding hydrocarbon surfactants, the reports of fluorocarbon surfactants have mostly concentrated on the partial or perfluorocarboxylic acids and their salts with monovalent ions as counterions,[27−31] while research on catanionic fluorocarbon/hydrocarbon surfactant mixtures is comparatively rare.[23,26]

In recent years, our group has described the phase behaviors of a series of salt-free catanionic surfactant systems composed of alkyltrimethylammonium hydroxide and fatty acids with different tails.[32−34] Fascinating self-assembly aggregates, e.g., wormlike micelles, onion phase, and lamellar structures, with remarkable viscoelasticity were observed. Herein, to perceive the influence of fluorocarbon chains on aggregation behaviors of catanionic surfactant systems, a perfluorononanoic acid ($C_8F_{17}COOH$) was mixed with tetradecyltrimethylammonium hydroxide (TTAOH) in aqueous solution to be compared with the hydrocarbon catanionic system $C_8H_{17}COOH/TTAOH/H_2O$. The results show that both systems have rich phase behaviors, but their aggregations are quite different. A phase transition from the planar lamellar phase ($L_{\alpha l}$ phase) to the vesicle phase ($L_{\alpha v}$ phase) in the $C_8H_{17}COOH/TTAOH/H_2O$ system was confirmed by ^2H NMR spectra. For the $C_8F_{17}COOH/TTAOH/H_2O$ system, at the $C_8F_{17}COOH$-rich side, a gel phase consisting of vesicles with crystalline state chains was demonstrated by freeze-fracture transmission electron microscopy (FF-TEM) observations and differential scanning calorimetry (DSC) measurements, which

* To whom correspondence should be addressed. E-mail: jhao@sdu.edu.cn. Fax: +86-531-88564750(o).
[†] Shandong University.
[‡] Chinese Academy of Sciences.

10.1021/jp104579h
Published on Web 09/24/2010

was rarely reported previously. Moreover, an ordinary $L_{\alpha v}$ phase consisting of polydisperse uni- and multilamellar vesicles was also observed. These results could provide further understanding of the phase characteristics and the difference between of hydrocarbon catanionic mixtures and hydro-/fluorocarbon ones, which may be useful to design these mixed systems to fit various requirements in academic research, material preparation, and industry applications, etc.

Experimental Section

Chemicals and Materials. Tetradecyltrimethylammonium bromide (TTABr) was purchased from Amresco Co. (Solon, OH, U.S.A.). Nonanoic acid ($C_8H_{17}COOH$, >98%) was purchased from Tokyo Chemical Industry CO., Ltd.. Perfluorononanoic acid ($C_8F_{17}COOH$, >98%) was purchased from Fluorochem Co. (Derbyshire, England). They were all directly used without further purification. D_2O (≥99.9%) was from Aldrich.

Preparation of Tetradecyltrimethylammonium Hydroxide (TTAOH). TTAOH stock solution was prepared from TTABr aqueous solution using a strong base anion exchanger (Ion exchanger III, Merck) at about 40 °C. TTAOH solution was detected by $AgNO_3$ solution with excess HNO_3 to confirm if Br^- ions were exchanged by OH^- absolutely ($Ag^+ + Br^- \rightarrow AgBr \downarrow$). The stock TTAOH solution was determined by acid−base titration with 0.10 mol·L^{-1} HCl to be 221.4 mmol·L^{-1}.

Phase Behavior Study. The total surfactant concentration was fixed to be 100.0 mmol·L^{-1} and the molar ratio of TTAOH, r_{TTAOH} ($r_{TTAOH} = n_{TTAOH}/(n_{fatty\ acid} + n_{TTAOH})$), is changeable. All samples were first ultrasonicated at 60 °C to accelerate the dissolution of surfactants. Then they were stored for at least 4 weeks at $T = 25.0 \pm 0.1$ °C to reach equilibrium. The phase diagrams were established on the basis of visual inspection with the help of crossed polarizers.

pH Measurements. The pH measurements were performed on a PHS-3C precision pH meter (China) at 25.0 ± 0.1 °C. Two-phase samples were equably stirred during the measurements.

Conductivity Measurements. The conductivity measurements were performed on a DDSJ-308A conductivity meter (China) at 25.0 ± 0.1 °C. Two-phase samples were equably stirred during the conductivity measurements. The conductivity value for each sample is the average of three measurements.

Textures of the Birefringent L_α phase Solutions. The birefringent L_α phase solutions were characterized on a Carl Zeiss Axioskop 40 light microscope (Jena, Germany) at 25.0 ± 0.1 °C.

^2H and ^{19}F NMR Measurements. All samples for ^2H and ^{19}F NMR measurements were first prepared in water and then were dried in a LGJ-10C freeze drier. After that, they were redissolved in D_2O with their original concentrations unchanged. ^2H and ^{19}F NMR spectra were recorded on a Bruker Avance 400 spectrometer equipped with pulse field gradient module (*Z* axis) using a 5 mm BBO probe. All the experiments were operated at 25.0 ± 0.1 °C.

Differential Scanning Calorimetry (DSC) Measurements. DSC measurements were operated on a DSC-Q10, TA Instruments (New Castle, PA, U.S.A.). Each sample was analyzed in an aluminum pan under a flow of nitrogen (20 mL/min) and heated at 5 °C/min from 20 to 80 °C, an empty aluminum pan was used as a reference.

Freeze-Fracture Transmission Electron Microscope (FF-TEM) Observations. The microstructure of the gel phase was characterized by FF-TEM observations. A small amount of sample was placed on a 0.1 mm thick copper disk covered with a second copper disk. Then the copper sandwich with the sample was plunged into liquid propane that had been cooled by liquid nitrogen to freeze. Fracturing and replication were carried out on a Balzers BAF-400D equipment at −140 °C at the Institute of Biophysics, CAS. Pt/C was deposited at an angle of 45°. The replicas were examined in a JEOL JEM-1400 electron microscope operated at 120 kV.

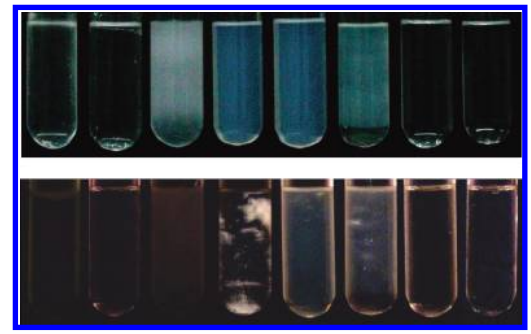

Figure 1. Phase behavior of the $C_8H_{17}COOH/TTAOH/H_2O$ system observed without (up) and with (below) crossed polarizers. The total surfactant concentration is 100.0 mmol·L^{-1}, $r_{TTAOH(CH)}$ from left to right is 0, 0.1, 0.25, 0.3, 0.4, 0.45, 0.5, and 0.6. $T = 25.0 \pm 0.1$ °C.

Cryo-Transmission Electron Microscope (Cryo-TEM) Observations. The samples were prepared in a controlled environment vitrification system (CEVS) at room temperature. First, about 5 μL sample solution was loaded onto a lacey support TEM grid held by a tweezer. The excess liquid was removed with a piece of blotting paper, leaving a thin film stretched over the holes. After about 10 s to relax any stress induced by the blotting, the samples were instantly frozen by plunging them into liquid ethane at its melting temperature (−183 °C). Then the vitrified specimens were inserted into liquid nitrogen and transferred to a cryogenic sample holder (Gatan 626). The observations of were carried out on a JEM 2200FS TEM (200 keV) at about −174 °C.

Rheological Measurements. Steady and dynamic rheological experiments were performed on a HAAKE RheoStress 6000 rheometer with a coaxial cylinder sensor system (Z41°Ti) for low viscous samples and cone−plate system (C35/1°Ti L07116) for samples with high viscosity. In oscillatory measurements, an amplitude sweep at a fixed frequency of 1.0 Hz was performed prior to the following frequency sweep to ensure the selected stress was in the linear viscoelastic region. Then the magnitudes of the complex viscosity $|\eta^*|$, the storage modulus G', and the loss modulus G'' were measured in the frequency range 0.01−10 Hz. The samples were measured at 25.0 ± 0.1 °C by using a Circulator HAAKE DC10 cyclic water bath (Karlsruhe, Germany).

Results and Discussion

1. $C_8H_{17}COOH/TTAOH/H_2O$ System. ***Phase Behavior.*** The total surfactant concentration is fixed to be 100.0 mmol·L^{-1} and the mixed ratio of $C_8H_{17}COOH$ to TTAOH is variable, which is marked by the mole fraction of TTAOH, $r_{TTAOH(CH)}$ ($r_{TTAOH(CH)} = n_{TTAOH}/(n_{C_8H_{17}COOH} + n_{TTAOH})$). The phase behavior and phase diagram are illustrated in Figures 1 and 2, respectively. The conductivity and pH data are included in the phase diagram. Nonanoic acid is an oily liquid and has very poor solubility in water at room temperature. One can see that at $r_{TTAOH(CH)} = 0$, nonanoic acid is on top of the aqueous solution (L_1 phase) due to its lower density than water. When $C_8H_{17}COOH$ and TTAOH are mixed together, with the increase

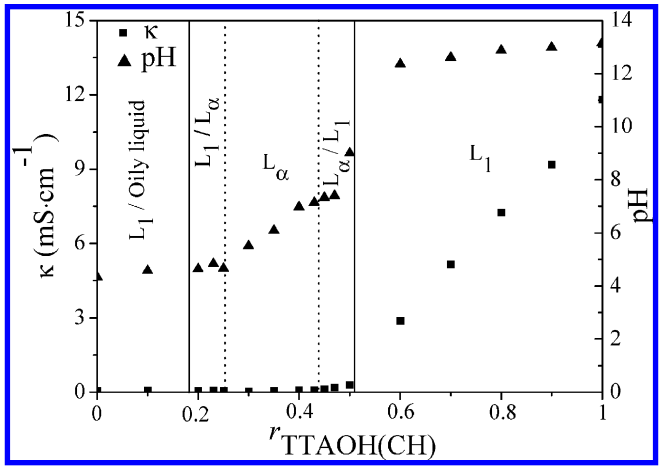

Figure 2. Phase diagram of the $C_8H_{17}COOH/TTAOH/H_2O$ system. The conductivity (■) and pH (▲) data are included in the phase diagram. The total surfactant concentration is 100.0 mmol·L^{-1}. T = 25.0 ± 0.1 °C.

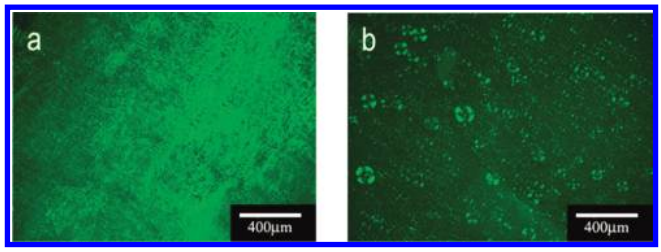

Figure 3. Polarized textures of two birefringent L_α phase samples at $r_{TTAOH(CH)}$ = 0.3 (a) and 0.4 (b).

of the TTAOH proportion, nonanoic acid is dissolved gradually and after a L_1/L_α phase region, a single L_α phase is observed from $r_{TTAOH(CH)}$ = 0.25 to 0.43. The L_α phase solutions are slightly turbid and bluish with obvious birefringence. From $r_{TTAOH(CH)}$ = 0.43 to 0.49, the macroscopic phase separation with a creamed L_α phase on top and an isotropic L_1 phase below is observed, indicating that the density of the L_1 phase is higher than that of L_α phase. After the two-phase region, from $r_{TTAOH(CH)}$ = 0.49 to 1.0, with TTAOH concentration increasing, the system reaches a single isotropic L_1 phase region with very low viscosity.

In our previous work, the property and function of a salt-free catanionic system, lauric acid (LA)/TTAOH/H_2O, were studied and the viscoelastic wormlike micellar phase and vesicle phase were obtained.[32,34] Compared with the LA/TTAOH/H_2O system, the $C_8H_{17}COOH/TTAOH/H_2O$ system consists of a fatty acid, nonanoic acid, which is a much shorter chain length to induce the different phase property. In LA/TTAOH/H_2O system, the single L_α phase exhibits at the TTAOH molar ratio from 0.43 to 0.46 with the same total surfactant concentration, c_{total} = 100.0 mmol·L^{-1}. Thus, it can be concluded that more amounts of fatty acids with shorter tails are needed to construct the bilayers than those of fatty acids with longer tails.

Figure 3 shows the textures of two L_α phase samples under crossed polarizers. The sample at $r_{TTAOH(CH)}$ = 0.3 has stripe textures (Figure 3a), while the sample at $r_{TTAOH(CH)}$ = 0.4 has cross-like spherulite textures (Figure 3b). Both polarized textures of the two samples demonstrate the existence of the lamellar phase.[35]

^{2}H NMR Measurements of the L_α Phase. The ^{2}H NMR experiments are useful and convenient for determining the phase behavior of surfactant solutions.[31,36,37] When the ^{2}H nucleus, with spin quantum number I = 1, is put in an external magnetic field, the spectrum of ^{2}H NMR depends on the interaction between the deuteron quadrupole moment and the electric field gradients around the nucleus. Moreover, the interaction is also dominated by the molecular orientation in relation to the magnetic field. For an isotropic solution, the properties are the same in all directions, so the interaction is averaged to zero due to the fast molecular motion and only a single sharp peak can be observed in the spectrum. In anisotropic solutions such as the lamellar or hexagonal phase, where the properties vary with different directions, the deuteron should result in the nonzero average of the interactions; therefore, doublet quadrupole splitting can be observed by ^{2}H NMR operations. Thus, ^{2}H NMR spectra show different properties in different self-assembly solutions. One doublet splitting peak can be observed in a lamellar or a hexangular liquid crystalline phase with different splitting values. For the L_3 phase (sponge phase) and cubic liquid crystalline phase, there is no splitting but a single peak in the ^{2}H NMR spectra. For the L_α phase aqueous solutions, it is very different for the $L_{\alpha l}$ phase (planar lamellar phase) and $L_{\alpha v}$ phase (vesicle phase). The $L_{\alpha l}$ phase solutions are long-range ordered macroscopically anisotropic systems. When H_2O is replaced by D_2O to prepare the samples, D_2O molecules at the interface of the planar surfactant bilayers show macroscopic anisotropy and doublet quadrupole splitting can be observed, inducing the splitting peaks in ^{2}H NMR spectra. However, for the $L_{\alpha v}$ phase, the solutions are composed of closed vesicle bilayers and D_2O molecules at the interface of bilayers exhibit only local anisotropy, which induces the interneutralization between the deuterium nuclei and the electric field. Thus, only single peaks appear in ^{2}H NMR spectra of $L_{\alpha v}$ phase solutions.

Figure 4 shows the ^{2}H NMR spectra of two L_α phase samples at $r_{TTAOH(CH)}$ = 0.3 and 0.4, respectively. When $r_{TTAOH(CH)}$ = 0.3, one can see two equally splitting peaks, indicating the existence of an anisotropic $L_{\alpha l}$ phase. While when $r_{TTAOH(CH)}$ increases to 0.4, only a single sharp peak is observed, implying the transition from $L_{\alpha l}$ phase to $L_{\alpha v}$ phase with the increase of TTAOH proportion. The phase transition should be ascribed to the repulsion between the bilayer charges. Nonanoic acid has an ionization equilibrium in aqueous solution, i.e., $C_8H_{17}COOH \rightleftharpoons C_8H_{17}COO^- + H^+$. With the increase of TTAOH amount, from $r_{TTAOH(CH)}$ = 0.3 to 0.4, pH values of the L_α phase solutions increase, as shown in Figure 2, indicating that the ionization equilibrium moves to form more $C_8H_{17}COO^-$. Due to the participation of $C_8H_{17}COO^-$ in bilayers, the charge density of the bilayers increases, which results in the bilayers to bend and close to form vesicles under the driving of electrostatic repulsions.

Rheological Properties. Dynamic rheological results of two L_α phase samples at $r_{TTAOH(CH)}$ = 0.3 and 0.4 are shown in Figure 5a,b, respectively. For the two samples, both of the elastic modulus G' and the viscous modulus G'' are very low and increase with the oscillatory frequency. Moreover, $|\eta^*|$ values are also very low. The results show that the two L_α phase samples do not present viscoelastic properties in the $C_8H_{17}COOH/TTAOH/H_2O$ system. A trend of the intersection of G' and G'' can be observed at high oscillatory frequency (more than 10 Hz), which is too fast to be measured accurately, indicating a very short stress relaxation time (τ_R). In our previous report of the LA/TTAOH/H_2O system, the L_α phase and wormlike micellar phase obtained were rather viscoelastic,[32] which was very different from the present system. These results of the $C_8H_{17}COOH/TTAOH/H_2O$ and LA/TTAOH/H_2O systems demonstrate that rheological properties are affected by the chain length of the surfactants.

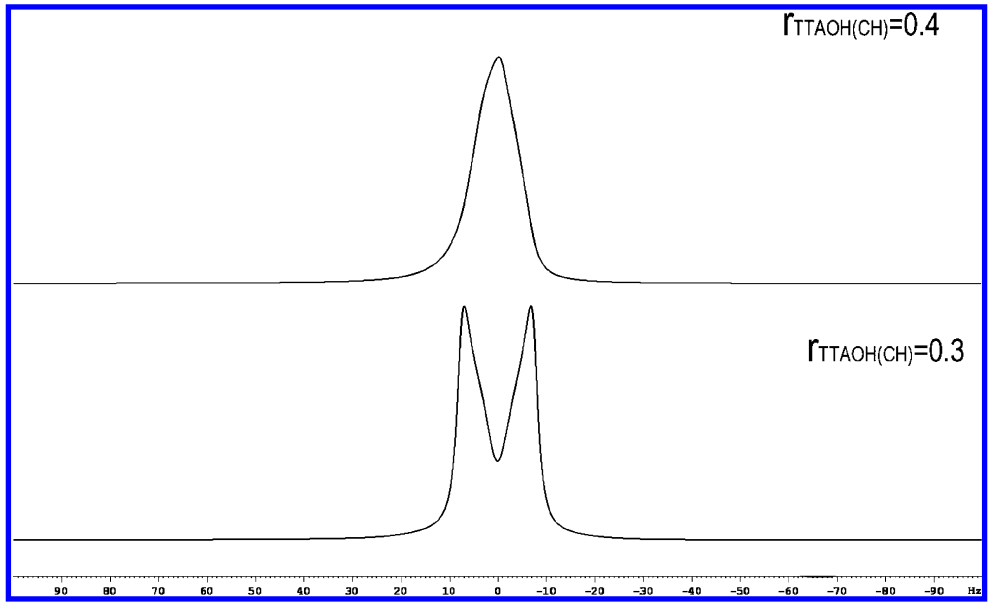

Figure 4. ^2H NMR spectra of the two L_α phase samples at $r_{TTAOH(CH)} = 0.3$ and 0.4. $T = 25.0 \pm 0.1$ °C.

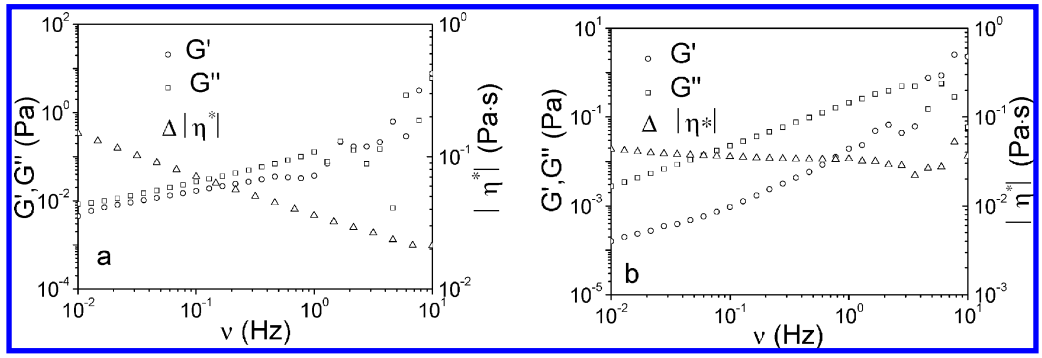

Figure 5. Oscillatory rheological data of two L_α phase samples at $r_{TTAOH(CH)} = 0.3$ (a) and 0.4 (b). $T = 25.0 \pm 0.1$ °C.

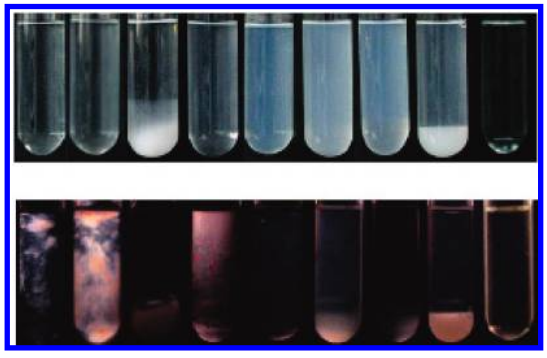

Figure 6. Typical sample photos of $C_8F_{17}COOH/TTAOH/H_2O$ mixtures without (up) and with (below) crossed polarizers. The total surfactant concentration is 100.0 mmol·L^{-1}, $r_{TTAOH(CF)}$ from left to right is 0, 0.1, 0.3, 0.4, 0.5, 0.55, 0.6, 0.7, and 1. $T = 25.0 \pm 0.1$ °C.

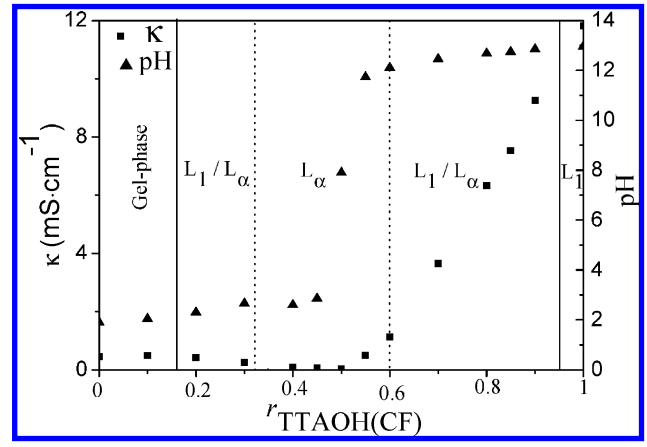

Figure 7. Phase diagram of the $C_8F_{17}COOH/TTAOH/H_2O$ system at $T = 25.0 \pm 0.1$ °C. Conductivity (■) and pH (▲) data are included in the phase diagram.

2. $C_8F_{17}COOH/TTAOH/H_2O$ System. ***Phase Behavior.*** Compared with the $C_8H_{17}COOH/TTAOH/H_2O$ system, the phase behavior of $C_8F_{17}COOH/TTAOH/H_2O$, as shown in Figure 6, is very different and interesting because of the different properties of fluorocarbon and hydrocarbon chains. The phase diagram including conductivity and pH data is shown in Figure 7. Without TTAOH, 100.0 mmol·L^{-1} perfluorononanoic acid solution is a gel phase with obvious birefringence and viscoelasticity, which will be discussed in a separate report in detail. When perfluorononanoic acid is replaced by TTAOH gradually, at different ratios of $r_{TTAOH(CF)}$ ($r_{TTAOH(CF)} = n_{TTAOH}/(n_{C_8F_{17}COOH} + n_{TTAOH})$), different phase regions can be observed. From $r_{TTAOH(CF)} = 0$ to 0.16, the samples are single transparent birefringent gel phase solutions consisting of packed vesicles formed by crystalline chains, which is demonstrated by DSC measurements and FF-TEM observation. Within the region from $r_{TTAOH(CF)} = 0.16$ to 0.33, the macroscopic phase separation with an isotropic L_1 phase on top and the L_α phase at bottom can be observed, indicating that the density of the L_α phase is higher than that of the L_1 phase. After the two-phase region, from $r_{TTAOH(CF)} = 0.33$ to 0.60, a single birefringent L_α phase region appears, which is confirmed to be an $L_{\alpha v}$ phase by cryo-TEM

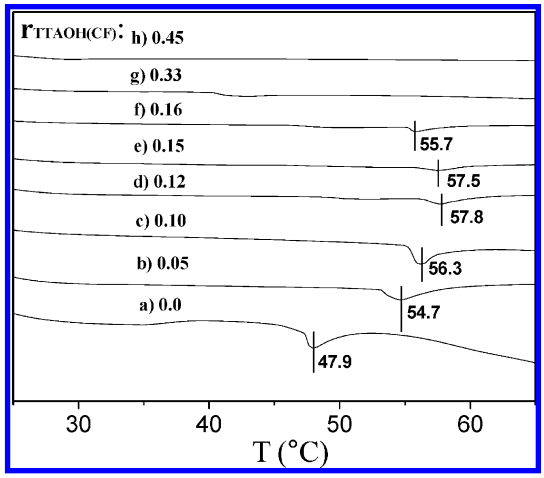

Figure 8. DSC curves of samples at $r_{TTAOH(CF)} = 0$ (a), 0.05 (b), 0.10 (c), 0.12 (d), 0.15 (e), 0.16 (f), 0.33 (g), and 0.45 (h). The total surfactant concentration is 100.0 mmol·L^{-1}.

determination and ^{2}H NMR measurements. When $r_{TTAOH(CF)}$ continues to increase, from $r_{TTAOH(CF)} = 0.60$ to 0.96, another macroscopic phase separation occurs with a creamed L_α phase at bottom and an isotropic L_1 phase on top. Finally, from $r_{TTAOH(CF)} = 0.96$ to 1, a very narrow region of single isotropic L_1 phase is observed.

DSC Measurements. Figure 8 shows DSC results of the gel phase and $L_{\alpha v}$ phase (i.e., L_α phase in Figure 7 consisting of vesicles) samples. The transition temperatures of the surfactant chains from crystalline state to liquid state can be obtained. Perfluorononanoic acid can dissociate completely into surfactant anions and H^+ below its cmc (2.75 mmol·L^{-1}) in aqueous solutions.[24] At concentrations above cmc, e.g., 100.0 mmol·L^{-1}, perfluorononanoic acid cannot dissolve at room temperature because of the high Krafft point, 48.3 °C.[27] However, when heated to above 50 °C under stirring, a birefringent vesicle solution can be obtained. The solution transforms into gel when it is cooled to room temperature. Figure 8a shows that the transition of fluorocarbon chains from crystalline state to liquid state occurs at 47.9 °C, which is very close to the Krafft point. When TTAOH is added, the transition temperature increases at first, as shown in Figures 8a−d, and then decreases with the further increase of TTAOH fraction, as shown in Figure 8d−f. This phenomenon might be attributed to two factors: one is the electrostatic interaction between $C_8F_{17}COO^-$ and TTA^+, which leads to the increase of chain-melting temperature; the other is the "softer" TTA^+ chains, having the chain-melting point below room temperature. Thus, the transition temperature is the integrative result of the two factors. In the $L_{\alpha v}$ phase region, one cannot observe the chain-melting process above 20 °C, as shown in Figure 8g,h, indicating the liquid state of the ion-pair surfactant chains at room temperature.

^{19}F and ^{2}H NMR Measurements. Fontell et al. investigated the phase equilibria of two-component systems of perfluorononanoic acid and its salts in aqueous solutions between 20 and 100 °C.[38] However, in their report only solutions below 0.2 wt % can be obtained. While in our study, for the perfluorononanoic acid aqueous solution above cmc, 100.0 mmol·L^{-1} (4.4 wt %), vesicles form at high temperature (above 50 °C). When cooled to room temperature, the liquid state chains freeze to crystalline state. Thus, the gel phase at the region from $r_{TTAOH(CF)} = 0$ to 0.16 is composed of vesicles with the bilayers formed by crystalline state chains. Compared with the corresponding hydrocarbon ones, fluorocarbon chains are more hydrophobic and rigid, which leads to the preference of the aggregates with less curvature or elongation, i.e., vesicles, lamellar structures, or wormlike micelles.[39]

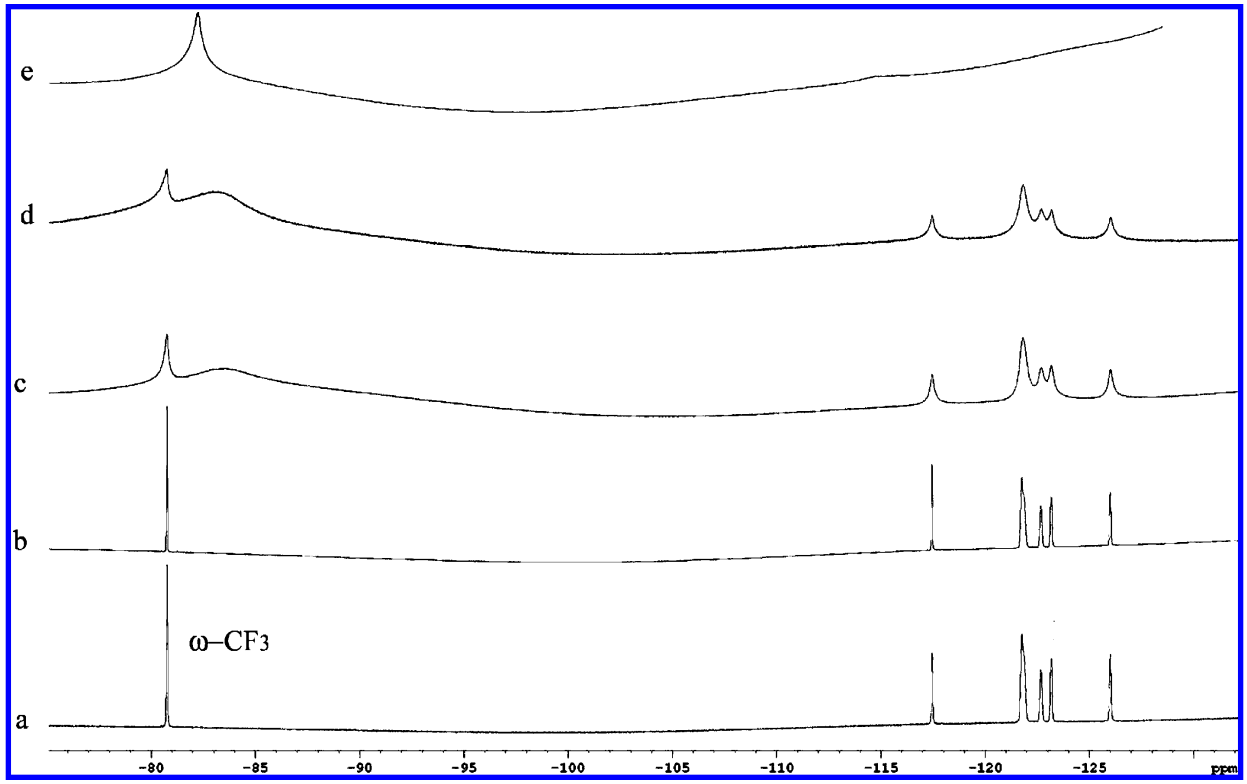

Figure 9. ^{19}F NMR spectra of $C_8F_{17}COOH$ in D_2O at different concentrations (mmol·L^{-1}): (a) 0.086 (below cmc), (b) 2.75 (at cmc), (c) 80.0 (gel phase), and (d) 100.0 (gel phase). Spectrum e is the sample at $r_{TTAOH(CF)} = 0.45$ with the total concentration of 100.0 mmol·L^{-1}. T = 25.0 ± 0.1 °C.

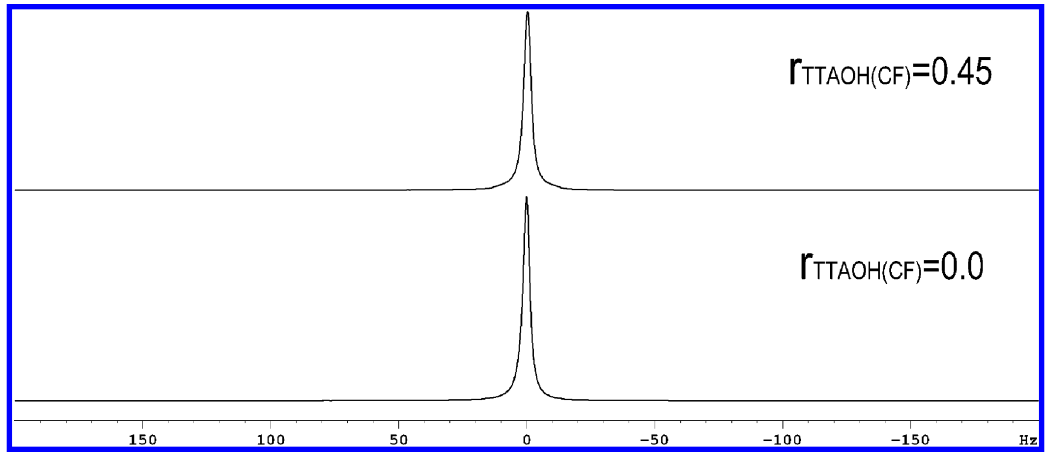

Figure 10. ^2H NMR spectra of samples at $r_{TTAOH(CF)} = 0$ and 0.45. $T = 25.0 \pm 0.1$ °C.

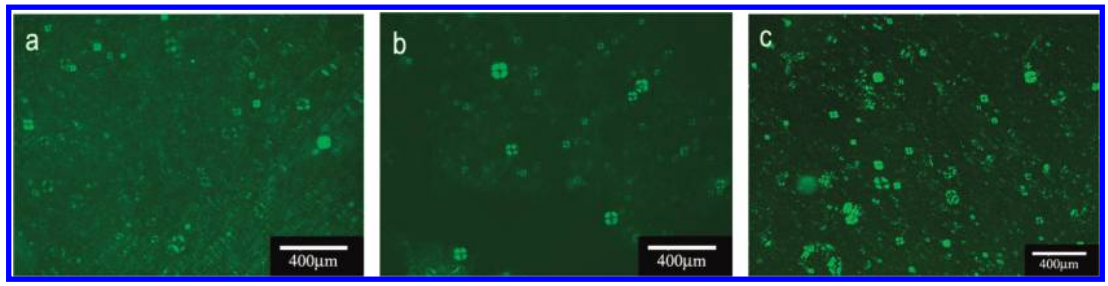

Figure 11. Polarized micrographs of three samples at $r_{TTAOH(CF)} = 0$ (a), 0.16 (b), and 0.45 (c). The total surfactant concentration is 100.0 mmol·L^{-1}.

The ^{19}F NMR spectra of $C_8F_{17}COOH$ at different compositions are shown in Figure 9a−d. In the monomer case, i.e., below its cmc, as shown in Figure 9a,b, the mobility of fluorocarbon chains is free, inducing the high resolution of ^{19}F NMR signals of different groups. When the concentration of $C_8F_{17}COOH$ is above its cmc, for gel phase samples, as shown in Figure 9c,d, the ^{19}F NMR signals become broader and less resolvable. However, the chemical shifts are unchangeable except for the terminal methyl (ω-CF_3) group. The reason should be that the ^{19}F NMR signals of crystalline chains cannot be detected and we can only get the monomers' signal. Because the monomers' mobility is prohibited in the gel phase, the ^{19}F NMR signals are less resolvable. For ω-CF_3, it is interesting that two separated ^{19}F NMR peaks are observed. The probable reason should be that, in crystalline state chains, ω-CF_3 is freer than other fluoromethylene groups ($-CF_2-$) and more sensitive to detect. Therefore, two signals at −80.9 and −83.2 ppm for the ω-CF_3 group are obtained, belonging to monomers and crystalline state chains, respectively. The separated NMR signals for one component with different existent forms have been reported.[28,40] For the $L_{\alpha v}$ phase sample with $r_{TTAOH(CF)} = 0.45$ (Figure 9e), only one broad peak for the ω-CF_3 group is detected. Similar behavior in other fluorocarbon/hydrocarbon catanionic surfactant systems was reported in our previous work.[41] This may be ascribed to two aspects: One is that in catanionic surfactant systems, the monomer concentration is much lower than that of individual surfactant due to the formation of surfactant ion pairs.[4] The other is that the mobility of fluorocarbon chains is prohibited around hydrocarbon chains.

Figure 10 shows the ^2H NMR spectra of two samples at $r_{TTAOH(CF)} = 0$ and 0.45. Only a single peak appears in the ^2H NMR spectraum for each sample, indicating a zero average of the quadrupole couplings between the ^2H nuclei and the electric field gradient. Thus, from ^2H NMR spectra we can also conclude the formation of the vesicle-formed gel phase and the $L_{\alpha v}$ phase (vesicle phase) of the two samples, which can be demonstrated by FF-TEM and Cryo-TEM images below.

Images of the Gel Phase and $L_{\alpha v}$ Phase. Figure 11 shows the polarized micrographs of two gel phase and an $L_{\alpha v}$ phase samples, in which the cross-like spherulite textures are clearly observed in all samples, indicating the existence of the lamellar structures.[35] Further characterizations are carried out by FF-TEM and cryo-TEM images, as shown in Figure 12. Figure 12a,b show that the gel phase samples are composed of polydisperse unilamellar vesicles. The $L_{\alpha v}$ phase sample at $r_{TTAOH(CF)} = 0.45$ consists of polydisperse vesicles including ordinary and elongated ones, as shown in Figure 12c. Most of the vesicles are unilamellar vesicles except very few bilamellar ones. The elongated vesicles demonstrate the flexibility of the vesicle bilayers.

Rheological Properties. Figure 13a,b shows the dynamic rheological properties of gel phase and $L_{\alpha v}$ phase samples. The gel phase samples at $r_{TTAOH(CF)} = 0$ and 0.16 have similar rheological properties and show high viscoelasticity. The elastic modulus G' of the both samples are higher than the viscous modulus G'', showing the elasticity dominating property, which are the typical characteristics of gels.[42,43] In the $L_{\alpha v}$ phase region, the rheological property is very different from that of the gel phase. At $r_{TTAOH(CF)} = 0.4$, as shown in Figure 13c, G' is lower than G'' at low oscillatory frequency and they intersect at a certain frequency. At $r_{TTAOH(CF)} = 0.45$, as shown in Figure 13d, both G' and G'' are much lower compared with those at $r_{TTAOH(CF)} = 0.4$, and the intersection of G' and G'' cannot be found within the frequency measured, implying a very weak viscoelasticity and a very fast relaxation process. From further study, one can find that G', G'', and $|\eta^*|$ all decrease with the increase of $r_{TTAOH(CF)}$, namely, the

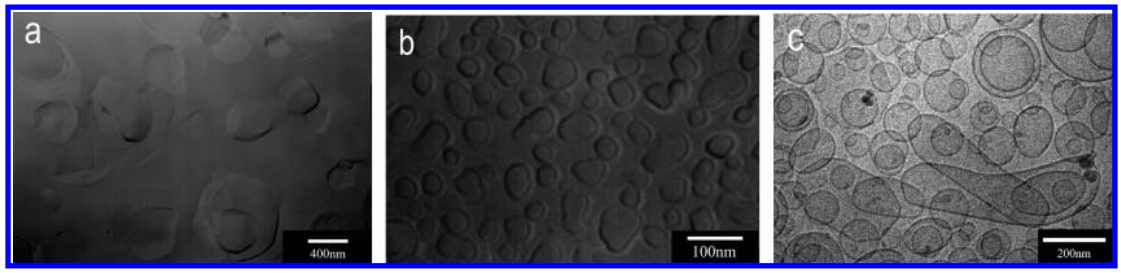

Figure 12. FF-TEM images of two gel phase samples at $r_{TTAOH(CF)} = 0$ (a) and 0.16 (b) and the cryo-TEM image (c) of sample at $r_{TTAOH(CF)} = 0.45$. The total surfactant concentration is 100.0 mmol·L^{-1}.

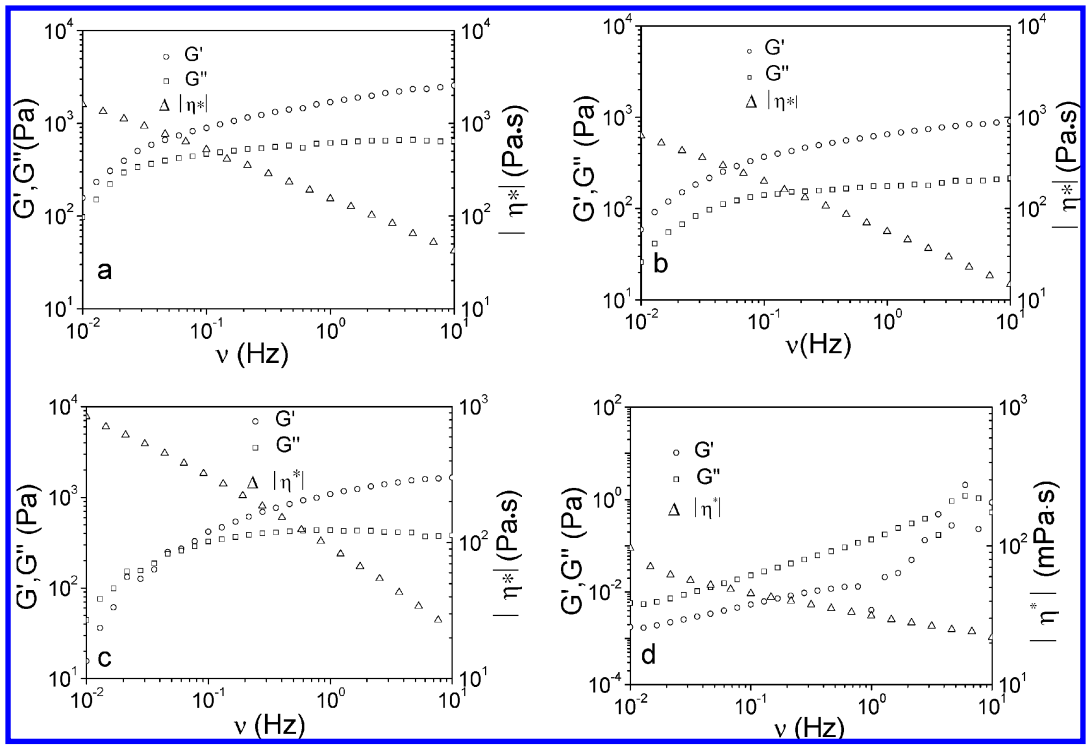

Figure 13. Oscillatory shear rheograms of four samples at $r_{TTAOH(CF)} = 0$ (a), 0.16 (b), 0.4 (c), and 0.45 (d). The total concentration of surfactants is 100.0 mmol·L^{-1}. $T = 25.0 \pm 0.1$ °C.

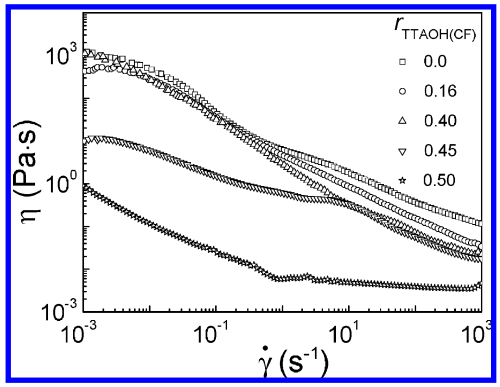

Figure 14. Steady shear rheograms of the selected samples at $r_{TTAOH(CF)} = 0$, 0.16, 0.40, 0.45, and 0.50. $T = 25.0 \pm 0.1$ °C.

viscoelasticity decreases with the decrease of the $C_8F_{17}COOH$ proportion. A similar phenomenon can also be observed in the steady shear results in Figure 14. With the increase of TTAOH proportion, the apparent viscosity decrease, which is in accordance with visual observations.

Conclusions

In summary, the phase behaviors of two catanionic surfactant systems, $C_8F_{17}COOH/TTAOH/H_2O$ and $C_8H_{17}COOH/TTAOH/H_2O$, were studied and showed remarkable differences because of the contrast between the fluorocarbon and hydrocarbon chains. The $C_8H_{17}COOH/TTAOH/H_2O$ system exhibits phase behavior similar to that of other fatty acid/$TTAOH/H_2O$ systems, while the phase regions are dependent on the chain length of the fatty acids. Within the L_α phase region, the transition from the $L_{\alpha l}$ phase to the $L_{\alpha v}$ phase appears due to the electrostatic repulsion between the bilayer charges, which increases with the increase of TTAOH proportion. The $C_8F_{17}COOH/TTAOH/H_2O$ system exhibits much higher capability of forming vesicle bilayers than that of the corresponding $C_8H_{17}COOH/TTAOH/H_2O$ system. At the $C_8F_{17}COOH$-rich side, a high viscoelastic gel phase consisting of crystalline vesicle bilayers is obtained at room temperature. With the increase of TTAOH proportion, the crystalline state vesicle bilayers melt to form liquid state vesicle bilayers. This phenomenon should be ascribed to the rigid structure and stronger hydrophobicity of the fluorocarbon chains, which prefer the formation of less curved aggregates and a high melting temperature. Considering that fluorinated

amphiphiles have great potential in industrial applications and have attracted great attention of academic study on aggregation behaviors, the results in our present results will provide useful information for the research and applications of fluorosurfactants.

Acknowledgment. This work is financially supported by the NSFC (Grant Nos. 20833010 and 20803045) and National Basic Research Program of China (973 Program, 2009CB930103).

References and Notes

(1) Bangham, A. D.; Horne, R. W. *J. Mol. Biol.* **1964**, *8*, 660.
(2) *Vesicles*; Rosoff, M., Ed.; Surfactant Science Series 62; Marcel Dekker, Inc.: New York, 1996.
(3) Kaler, E. W.; Murthy, A. K.; Rodriguez, B. E.; Zasadzinski, J. A. N. *Science* **1989**, *245*, 1371.
(4) Hao, J.; Hoffmann, H. *Curr. Opin. Colloid Interface Sci.* **2004**, *9*, 279.
(5) Kaler, E. W.; Herrington, K. L.; Murthy, A. K. *J. Phys. Chem.* **1992**, *96*, 6698.
(6) Herrington, K. L.; Kaler, E. W.; Miller, D. D.; Zasadzinski, J. A.; Chiruvolu, S. *J. Phys. Chem.* **1993**, *97*, 13792.
(7) Yatcilla, M. T.; Herrington, K. L.; Brasher, L. L.; Kaler, E. W.; Chiruvolu, S.; Zasadzinski, J. A. *J. Phys. Chem.* **1996**, *100*, 5874.
(8) Iampietro, D.; Kaler, E. W. *Langmuir* **1999**, *15*, 8590.
(9) Koehler, R. D.; Raghavan, S. R.; Kaler, E. W. *J. Phys. Chem. B* **2000**, *104*, 11035.
(10) Raghavan, S. R.; Fritz, G.; Kaler, E. W. *Langmuir* **2002**, *18*, 3797.
(11) Schubert, B. A.; Kaler, E. W.; Wagner, N. J. *Langmuir* **2003**, *19*, 4079.
(12) González, Y. I.; Stjerndahl, M.; Danino, D.; Kaler, E. W. *Langmuir* **2004**, *20*, 7053.
(13) Zemb, Th.; Dubois, M.; Demé, B.; Gulik-Krzywicki, Th. *Science* **1999**, *283*, 816.
(14) Dubois, M.; Demé, B.; Gulik-Krzywicki, Th.; Dedieu, J. C.; Vautrin, C.; Désert, S.; Perez, E.; Zemb, Th. *Nature* **2001**, *411*, 672.
(15) Dubois, M.; Lizunov, V.; Meister, A.; Gulik-Krzywicki, Th.; Verbavatz, J. M.; Perez, E.; Zimmerberg, J.; Zemb, Th. *Proc. Natl. Acad. Sci. U.S.A.* **2004**, *101*, 15082.
(16) Song, A.; Dong, S.; Jia, X.; Hao, J.; Liu, W.; Liu, T. *Angew. Chem., Int. Ed.* **2005**, *44*, 4018.
(17) Jokela, P.; Jönsson, B.; Khan, A. *J. Phys. Chem.* **1987**, *91*, 3291.
(18) Hao, J.; Liu, W.; Xu, G.; Zheng, L. *Langmuir* **2003**, *19*, 10635.
(19) Li, H.; Jia, X.; Li, Y.; Shi, X.; Hao, J. *J. Phys. Chem. B* **2006**, *110*, 68.
(20) Li, H.; Hao, J. *Chem. Lett.* **2007**, *36*, 702–703.
(21) Li, H.; Xin, X.; Kalwarczyk, T.; Kalwarczyk, E.; Niton, P.; Hołyst, R.; Hao, J. *Langmuir* 2010, DOI: 10.1021/la1029068.
(22) Alvaro, S. F.; Francisco, G. C. *Biochem. J.* **1992**, *285*, 373–376.
(23) Li, X.; Dong, S.; Jia, X.; Song, A.; Hao, J. *Chem.—Eur. J.* **2007**, *13*, 9495.
(24) Hoffmann, H.; Würtz, J. *J. Mol. Liq.* **1997**, *72*, 191.
(25) Weiss, M. T.; Narayanan, T.; Gradzielski, M. *Langmuir* **2008**, *24*, 3759.
(26) Long, P.; Hao, J. *Soft Matter* 2010, DOI: 10.1039/c0sm00395f.
(27) Kunieda, H.; Shinoda, K. *J. Phys. Chem.* **1976**, *80* (22), 2468.
(28) Guo, W.; Brown, T. A.; Fung, B. M. *J. Phys. Chem.* **1991**, *95*, 1829.
(29) Thünemann, A. F.; Schnablegger, H. *Langmuir* **1999**, *15*, 5426.
(30) Amato, M. E.; Caponetti, E.; Martino, D. C.; Pedone, L. *J. Phys. Chem. B* **2003**, *107*, 10048.
(31) Dong, S.; Xu, G.; Hoffmann, H. *J. Phys. Chem. B* **2008**, *112*, 9371.
(32) Li, H.; Hao, J. *J. Phys. Chem. B* **2008**, *112*, 10497.
(33) Yuan, Z.; Hao, J. *J. Phys. Chem. B* **2008**, *112*, 1414.
(34) Li, H.; Hao, J. *J. Phys. Chem. B* **2009**, *113*, 2371.
(35) Horbaschek, K.; Hoffmann, H.; Thunig, C. *J. Colloid Interface Sci.* **1998**, *206*, 439.
(36) Khan, A.; Fontell, K.; Lindblom, G.; Lindman, B. *J. Phys. Chem.* **1982**, *86*, 4266.
(37) Jokela, P.; Jönsson, B.; Khan, A. *J. Phys. Chem.* **1987**, *91*, 3291.
(38) Fontell, K.; Lindman, B. *J. Phys. Chem.* **1983**, *87*, 3289.
(39) Matsuoka, K.; Moroi, Y. *Curr. Opin. Colloid Interface Sci.* **2003**, *8*, 227.
(40) Bossev, D. P.; Matsumoto, M.; Nakahara, M. *J. Phys. Chem. B* **1999**, *103*, 8251.
(41) Dong, S.; Song, A.; Hao, J. *Colloids Surf. A* **2010**, *359*, 53.
(42) Rakesh, K.; Gokul, C. K.; Lior, Z.; Dganit, D.; Srinivasa, R. R. *Langmuir* **2007**, *23*, 12849.
(43) Jiang, W.; Wu, Z.; Hao, J. *Langmuir* **2008**, *24*, 3150.

JP104579H